ADVANCED ELECTRONIC MATERIALS Open Access
www.advelectronicmat.de

Organic Mixed Ionic Electronic Conductor Nanochannels for Vertical Electrochemical and Ionic Transistors

Chenhong Zhang, Lorenzo Margotti, Francesco Decataldo, Alberto Piccioni, Hongzhi Wang, Beatrice Fraboni, Yaogang Li, and Tobias Cramer**

Thin films of organic mixed ionic electronic conductors (OMIECs) constitute the functional layer in organic electrochemical transistors (OECTs), organic bioelectronic transducers and other ionic-electronic devices. The thin-film configuration constrains devices to be fabricated on impermeable substrates in the form of 2D microstructures with lateral electrodes to drive an electronic current through the thin film. In order to alleviate such constraints, novel OMIEC deposition methods are needed that produce alternatives to thin-film devices and that are compatible with permeable substrates and electronic transport in the vertical direction. Here OMIECs filled nanoporous membranes are introduced as functional layer in devices with mixed ionic electronic transport. Electropolymerization of ethylenedioxythiophene (EDOT) monomers is used to fabricate OMIEC filled nanochannels. Electronic and ionic transport through such nanochannels are investigated and modulation of electronic as well as ionic carrier density by action of a third gate electrode is demonstrated. The novel OMIEC nanochannels enable the fabrication of vertical OECTs with high transconductance and organic ionic transistors using only additive fabrication methods.

1. Introduction

Microelectronic devices and circuits that integrate ionic and electronic current transport[1] are currently at the focus of research due to their relevance for bioelectronic sensors and actuators[2] and high transconductance transistors.[3] A widely studied example are organic electrochemical transistors (OECTs)[4] that rely on a thin film of organic mixed ionic and electronic conductor (OMIEC) such as the polymer poly(3,4-ethylenedioxythiophene) polystyrene sulfonate (PEDOT:PSS). The thin film constitutes the so-called transistor channel and is in contact with an ionically conducting electrolyte forming the transistor gate. Changes in gate potential caused by externally applied voltage, ionic currents or electrochemical Nernst potentials, alter the OMIEC electronic carrier concentration and hence also the OECT channel conductivity. Accordingly, OECTs work as an amplifier as small ionic or electrochemical signals in the gate can cause a large electronic current response in the transistor channel.[5,6] Optimized OECT response depends on the properties of the OMIEC channel material (electronic and ionic mobility, volumetric capacitance) and the OECT device geometry.[7] State-of-the-art performance with high transconductance and fast response is obtained in thin-film devices with micrometric channel dimensions.[8] However, such a thin-film device configuration has some drawbacks. First, it relies on micrometric patterning by photolithography that is difficult to integrate with low-cost printing based fabrication techniques. Second, it requires impermeable substrates for the OMIEC thin film deposition and generally imposes a 2D geometry to OECT devices. To overcome these limitations and to provide novel perspectives for OECTs, alternative fabrication techniques and channel geometries such as vertical transistor designs[9] are needed. The goal is to achieve micrometric OMIEC based transistor channels with sustainable additive fabrication methods.

Electropolymerization is a well-established additive technique to deposit thin films of OMIECs from solutions containing conjugated monomers such as ethylenedioxythiophene (EDOT) or polypyrrol (Py) and anions that enter the growing film as dopants.[10] The polymerization is driven by charge transfer from a metallic electrode allowing electrical control on the position and the amount of deposited polymer.[11] Electropolymerization has been exploited to fabricate the channel of macroscopic OECTs in planar[12] and recently also in vertical devices.[13,14] The technique is chemically versatile allowing for the incorporation of different doping anions[15] or selective binding sites

C. Zhang, H. Wang, Y. Li
State Key Laboratory for Modification of Chemical Fibers and Polymer Materials
College of Materials Science and Engineering
Donghua University
Renmin Road 2999, Shanghai 201620, P. R. China
E-mail: yaogang_li@dhu.edu.cn

L. Margotti, F. Decataldo, A. Piccioni, B. Fraboni, T. Cramer
Dipartimento di Fisica e Astronomia
Università di Bologna
Viale Berti Pichat 6/2, Bologna 40127, Italy
E-mail: tobias.cramer@unibo.it

The ORCID identification number(s) for the author(s) of this article can be found under https://doi.org/10.1002/aelm.202300762

DOI: 10.1002/aelm.202300762

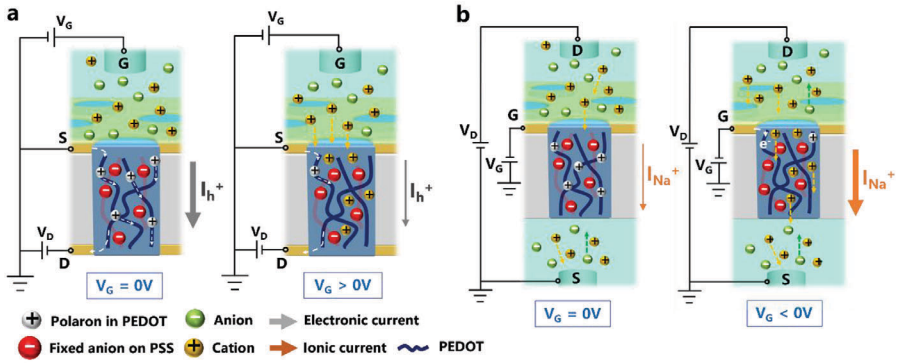

Figure 1. Concept of OMIEC nanochannel devices with electronic and ionic transport. a) Electronic transport in a vertical electrochemical transistor with open ($V_G = 0$ V) and closed ($V_G < 0$ V) nanochannel. The source-drain current I_h^+ relies on electronic hole carriers in the OMIEC channel. b) Ionic transport in a vertical ionic nanochannel transistor with gate-dependent ionic conductivity. Source and drain electrodes are salt bridges and permit only ionic source-drain currents I_{Na}^+.

in biosensors.[16] During electropolymerization, OMIEC films grow along the monomer concentration gradient which makes it difficult to obtain thin, high-performance OECT channels covering a dielectric substrate. Directed growth during electropolymerization was demonstrated with bipolar deposition techniques[17] or by template-based growth in confined geometries such as nanoporous aluminum oxide to yield conducting polymer nanotubes.[18,19]

Here we exploit electropolymerization to introduce a novel OECT channel geometry that provides an alternative to the thin film approach. We fabricate OMIEC nanochannels by EDOT electropolymerization into a nanoporous polycarbonate membrane. For different OMIEC compositions, we demonstrate the electronic and ionic conductivity of the nanochannels. With appropriate source and drain electrodes, the filled nanoporous membranes enable micrometric, vertical OECT structures fabricated without lithography showing state-of-the-art transconductance. The permeability of the nanochannels for ions and water is further exploited in novel device functionalities. As an example, we demonstrate the gating of ionic currents by an electronic gate potential in a device that we call an organic ionic transistor.

2. Results

2.1. Concept of Electronic and Ionic Transistors with Nanopore Channels

The structure and the modulation principle of the proposed vertical electronic and ionic transistors are introduced in **Figure 1**a,b. Both devices exploit as the key element a nanoporous membrane containing pores filled with OMIECs such as PEDOT:PSS or PEDOT:Cl. The two device types distinguish only in how the source and drain contacts are realized. In the electrochemical transistor the polymer channel conducts electronic hole carriers that are injected and extracted by the source and drain electrodes made of evaporated gold layers deposited on both sides of the nanoporous membrane. The electronic current is gated by ions entering the nanopore channel. At negative gate potential, cations accumulate in the nanopore channel and replace electronic hole carriers eventually switching off the electronic transistor current.

The vertical ionic transistor relies on an ionic current that passes through the nanopore (Figure 1b). Accordingly, source and drain electrodes correspond to electrolyte reservoirs present on both sides of the membrane. A potential difference between the reservoirs causes drift-diffusion of ions through the channel. We hypothesize that also in this case the ionic conductivity of the channel could be modulated by the electronic potential applied to the conducting polymer nanopore as it controls the number of mobile ions in the nanopore channel. For example for a PEDOT:PSS channel, a positive potential could cause the depletion of mobile cations, reducing the channel's ionic conductivity. In the following we describe first the fabrication of the OMIEC filled nanopores and then the two different measurement configurations to access electronic and ionic transport through the pores.

2.2. Electrodeposition of the Conducting Polymer Nanochannels

The fabrication of the OMIEC nanochannels relies on track-etched polycarbonate membranes with precisely controlled nanopore diameter and density as template.[20] **Figure 2**a introduces the fabrication procedure developed to obtain the vertical channel transistor structures. In the first step, a layer of gold with chromium adhesion layer is evaporated on one side of the insulating nanoporous membrane. The next steps realize the filling of the nanopores with conducting polymer using electropolymerization of EDOT. To guide the electropolymerization into the pores, the nanoporous membrane was laminated with the gold side onto a polydimethylsiloxane (PDMS) substrate. A low-power plasma treatment is used to render the nanopore membrane more hydrophilic. Subsequently, the membrane is put into contact with an aqueous solution containing the EDOT monomer and the ionic dopant (NaPSS or NaCl). Due to the laminated PDMS substrate, the solution enters only from the top side into the pores. The filling of the nanopores with solution is facilitated by ultrasound and elevated temperature (30 °C). The electropolymerization is driven by a potentiostat using the laminated gold layer as working electrode with Ag/AgCl reference and Pt-wire counter electrode. Conducting polymer deposition starts at the bottom of the nanopore where the edge of the gold layer is in direct contact with the EDOT containing electrolyte as shown

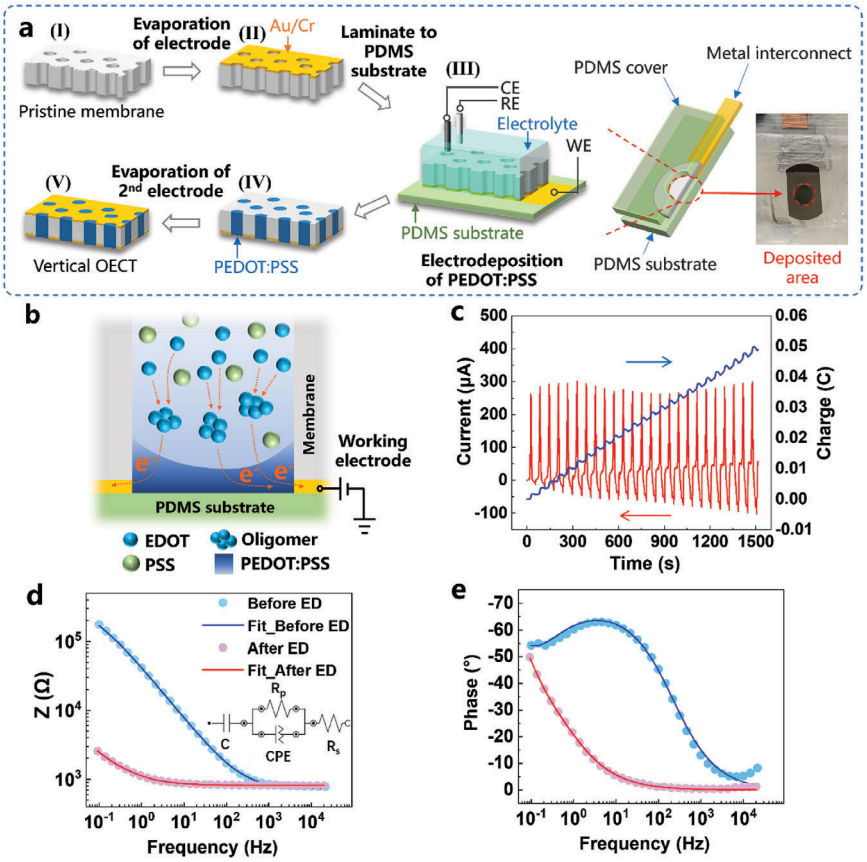

Figure 2. Fabrication of OMIEC filled nanoporous membranes by electrodeposition. a) Illustration of the sequence of fabrication steps b) Scheme showing the electropolymerization of PEDOT:PSS into the nanopore. c) Electrode current (red line) and accumulated charge (blue line) during electrodeposition of PEDOT:PSS into the nanoporous membrane. d,e) Electrical impedance spectroscopy of the nanoporous membrane before (blue) and after (pink) electropolymerization: d) magnitude and e) phase angle of impedance.

in Figure 2b. The electropolymerization is controlled by running voltammetry cycles (−0.3 to 1.2 V vs Ag/AgCl) as shown in Figure 2c. Such curves allow to monitor the progress of the electrodeposition in real time. The successful deposition of the conducting polymer shows a strong increase in current in the CV cycle at potentials > 1 V (Figure S1, Supporting Information). During each cycle a constant amount of charge is deposited causing a steady filling of the pores. Failures in membrane sealing or excessive polymer formation outside of pores are reported by a sudden increase in the deposited charge.[19] We found that the cut-off charge Q_c required to fill the nanopores can be estimated with the formula:

$$Q_c = \frac{V_{eff}\ \rho_{EDOT}}{M_{EDOT}} e\ N_A \quad (1)$$

Where ρ_{EDOT} is the density of EDOT, M_{EDOT} is the molar mass of EDOT, e is the elementary charge, and N_A is Avogadro's number. Here, $V_{eff} = A_s * \rho_p * A_p * l$ is the effective pore volume to be filled, A_s is the area of membrane surface in contact with solution (circular shape of 5 mm in diameter), ρ_p is the number density of the pores per area A_p is the area of a single pore, l is the thickness of the membrane.

Additionally, nanopore filling is monitored with electrochemical impedance spectroscopy (EIS). Figure 2d,e report the impedance modulus and phase spectra obtained before and after PEDOT:PSS electrodeposition combined with the equivalent circuit model and its fit to the data. One observes a significant reduction in impedance as a consequence of the PEDOT:PSS deposition. Only at high frequencies the impedance response is dominated by the ionic transport through the electrolyte. At lower frequencies, the capacitive interaction prevails and is combined in the model with a constant phase element to account for time constant dispersion due to transport through the nanopore. From the fit, we obtain specific capacitances of 16.3 ± 2.5 μF cm^{-2} for the gold surface and 39.4 ± 5.7 μF cm^{-2} for the filled PEDOT:PSS pores. The latter value translates into a volumetric capacitance of 39.4 ± 5.7 F cm^{-3} when taking the thickness of the nanoporous membrane into account and the pore density. The value agrees with the volumetric capacitance reported previously for PEDOT:PSS thin films.[21]

2.3. Morphology of the Conducting Polymer Nanopore Channels

Microscopic characterizations were performed to investigate the morphology of the nanopores filled with conducting polymer.

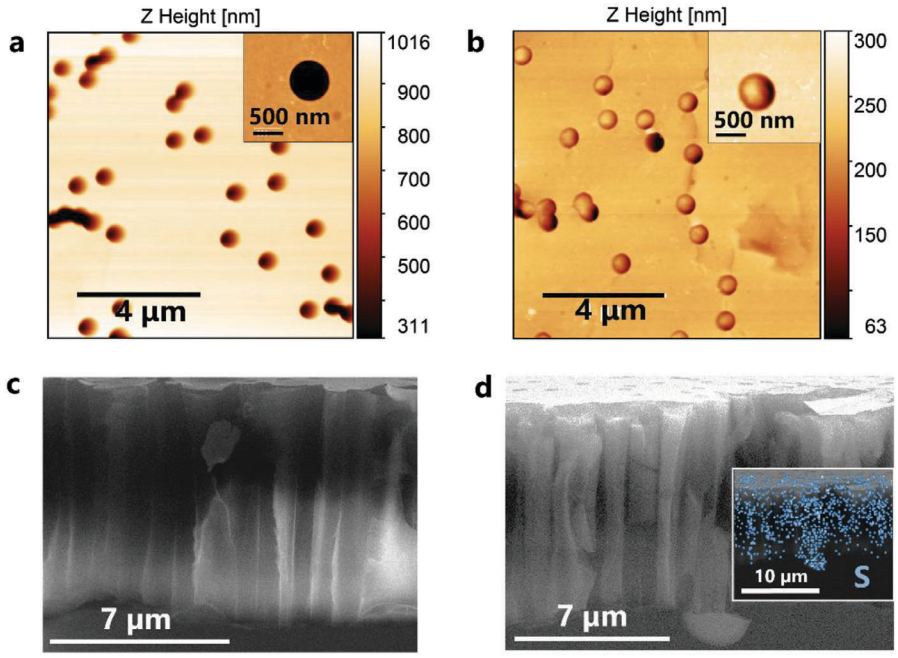

Figure 3. Morphological characterization of the porous membrane. AFM topography of a) the pristine membrane and b) the membrane deposited with PEDOT:PSS, the insets show the zoom of a single nanopore in each membrane. SEM images of the cross section of c) the pristine membrane and d) the membrane deposited with PEDOT:PSS, inset shows the EDX mapping analysis of sulfur.

Figure 3a,b compare the atomic force microscopy (AFM) topography of the gold covered nanoporous membrane before and after electrodeposition of PEDOT:PSS. The pristine membrane shows nanopore openings of 800±50 nm randomly distributed resulting in a density of 28 ± 0.7 pores per 100 µm^2. After electrodeposition, one observes that most of the nanopores are filled with polymer. No signs of polymer deposition could be detected outside the pore region. The occasional occurrence of empty nanopores is attributed to the presence of air bubbles at the bottom of the nanopore that inhibits contact between the solution and the gold electrode. Further confirmation of complete pore filling is obtained by scanning electron microscopy (SEM) performed on cross sections of pristine and filled membranes as reported in Figure 3c,d. The SEM images demonstrate the presence of additional material that fills the pores throughout the membrane thickness after electroplymerization. The inset shows the data from energy-dispersive X-ray (EDX) analysis confirming the presence of the element S throughout the membrane, which is unique to PEDOT:PSS and absent in the pristine polycarbonate of the membrane (detailed EDX data in Figure S2 and Table S1, Supporting Information).

2.4. Investigation of Electronic Transport through the OMIEC Filled Nanopores

Following the device concept reported in Figure 1a, the electronic transport through the nanopores is investigated in a vertical OECT structure. Fabrication of such a vertical OECT is completed by depositing a second gold layer on the top side of the membrane after the electrodeposition process. In this way, the device contains two gold layers that sandwich the nanoporous membrane acting as source and drain electrode. The device is put in contact with 0.1 M phosphate buffered saline (PBS) as electrolyte. A chlorinated silver wire is used to set the electrical potential of the electrolyte with respect to the membrane acting as a gate electrode in the OECT. The setup to measure the nanochannel current I_D as function of the gate potential V_G is reported in **Figure** 4a. The transfer characteristics obtained with this setup are shown in Figure 4b for different drain potentials. In all cases, the sweep of gate potential from −0.6 V to 0.8 results in a significant modulation of the drain current. At positive potentials the current is suppressed as electronic hole carriers in the organic semiconductor are replaced by cations entering the nanopore from the electrolyte (output characteristics in Figure S3, Supporting Information).

The reversible ionic gating of the nanopore electronic current is confirmed by the transients of drain current shown in Figure 4c. Applying rectangular potential pulses of 0.3 V to the gate causes a transient reduction in drain current that follows an exponential sawtooth shape with a characteristic time constant of τ = 0.39 ± 0.02 s. The time constant is in agreement with the RC time constant predicted from the EIS experiment (C = 1.1 ± 0.2 mF, R = 809 ± 60 Ω). We note that the slow response here is mainly attributed to the large capacitance of the device caused by the large area of the source and drain electrodes that contact many nanopores in parallel. Reducing the size of the evaporated electrodes would reduce the response time.

A significant advantage of the short and parallel nanochannels is the large transconductances of the vertical OECT as reported in Figure 4d as a function of different drain voltages. The maximum value of 5.6 mS at V_D = 0.7 V is comparable to values that were obtained in optimized thin film devices fabricated with photolithography.[5] Here transconductance is high due to

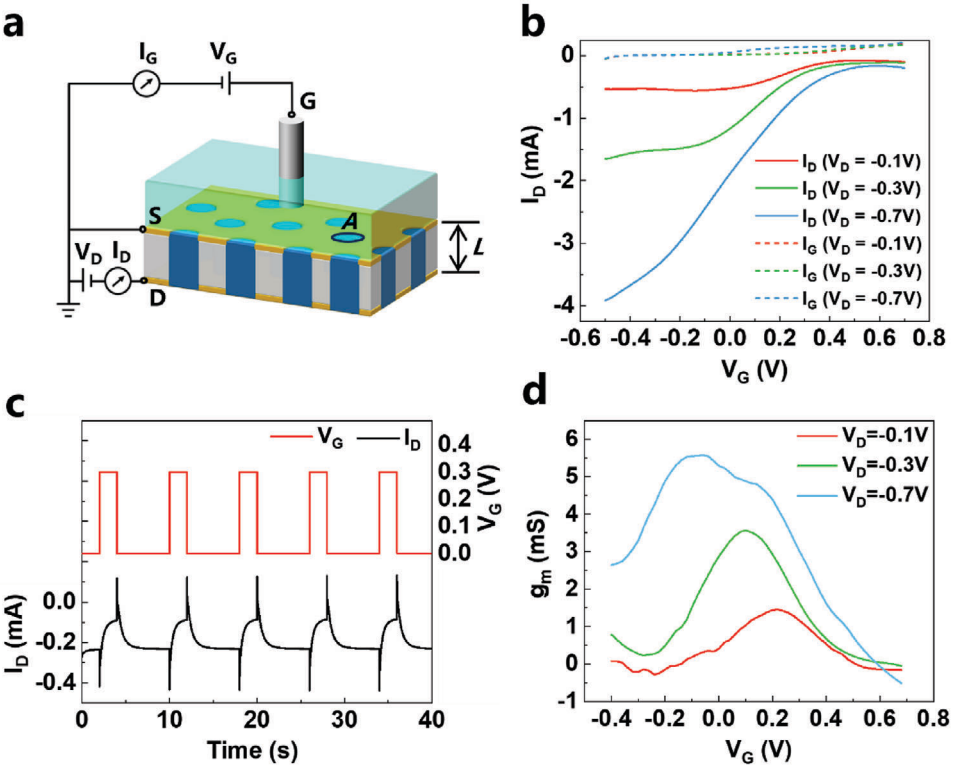

Figure 4. Investigation of electronic transport in OMIEC filled nanopores: a) Schematic of the vertical OECT based on the nanoporous membrane, the evaporated Au/Cr layers are used as the source and drain, and the PEDOT:PSS filled nanopores constitute the channel. The length (L) of the channel is equal to the thickness of the membrane, and the cross section area of the OECT channel is given by the sum of all the PEDOT:PSS nanochannels A contacted by the electrodes. b) Transfer characteristics measured at different drain voltages (V_D), including the curves of gate current (I_G) and drain current (I_D). c) Transients of drain current at $V_D = -0.1$ V. d) Transconductance with various drain voltages. All the measurements were carried out in the PBS electrolyte, an Ag/AgCl electrode was applied as the gate.

the channel geometry and we note that the charge transport properties of the nanochannels do not match to the thin film behavior observed in planar OECTs. From the transfer characteristics, we estimate an electronic mobility of (5.1 ± 0.42) x 10^{-3} cm^2 V^{-1} s^{-1} at $V_D = -0.7$ V for hole carriers in the nanochannels (Determination of mobility see Section S1, Supporting Information). In addition, one observes a maximum in transconductance at intermediate gate voltages and a reduction in transport occurs at negative gate voltages when strong accumulation occurs in the channel. These findings show that the transport is well defined in the nanochannels, but polymer morphology and contact properties can be further improved to maximize device properties.

2.5. Investigation of Ionic Transport through the OMIEC Filled Nanopores

The OMIEC filled nanoporous membrane enables experiments where the electrolyte is present on both sides of the membrane and the transfer of ions through the pores can be investigated as schematically shown in **Figure** 5a. We use salt bridges to inject and extract the ionic current from the electrolyte reservoirs above and below the membrane to not alter the ionic concentrations (see Experimental Section for details). For a sourced ionic current, we measure the voltage drop across the membrane with a four-point probe measurement scheme. A voltage source is used to apply the gate potential to the evaporated gold film contacting the OMIEC filled nanopores in the membrane that separates the two electrolyte reservoirs. The obtained current-voltage characteristics for PEDOT:PSS filled nanopores are shown in Figure 5b. For comparison the *I–V* characteristics of the membrane with empty pores are also presented. One observes that in all cases the membrane remains permeable for ionic currents. However, the presence of PEDOT:PSS increases the slope of the curves: for a given current, a higher voltage drop across the membrane is observed. Accordingly, the ionic conductivity is reduced for PEDOT:PSS filled nanopores. The application of a gate potential does not alter the slope of the current voltage curves and only contributes a small offset that is attributed to gate leakage currents. We conclude that the ionic conductivity is not significantly modulated in PEDOT:PSS nanopores although electronic hole charges are replaced by cations. We suggest that this finding is caused by the high ion concentration in PEDOT:PSS due to the polyanion PSS. Already at 0 V gate, only a smaller part of the anionic charges is counterbalanced by hole charges while the majority of PSS is coordinated to sodium ions in the polymer. Accordingly at all gate potentials, a large amount of sodium ions is present in the pores and the smaller modulation due to gating has no significant effect on ionic conductivity.

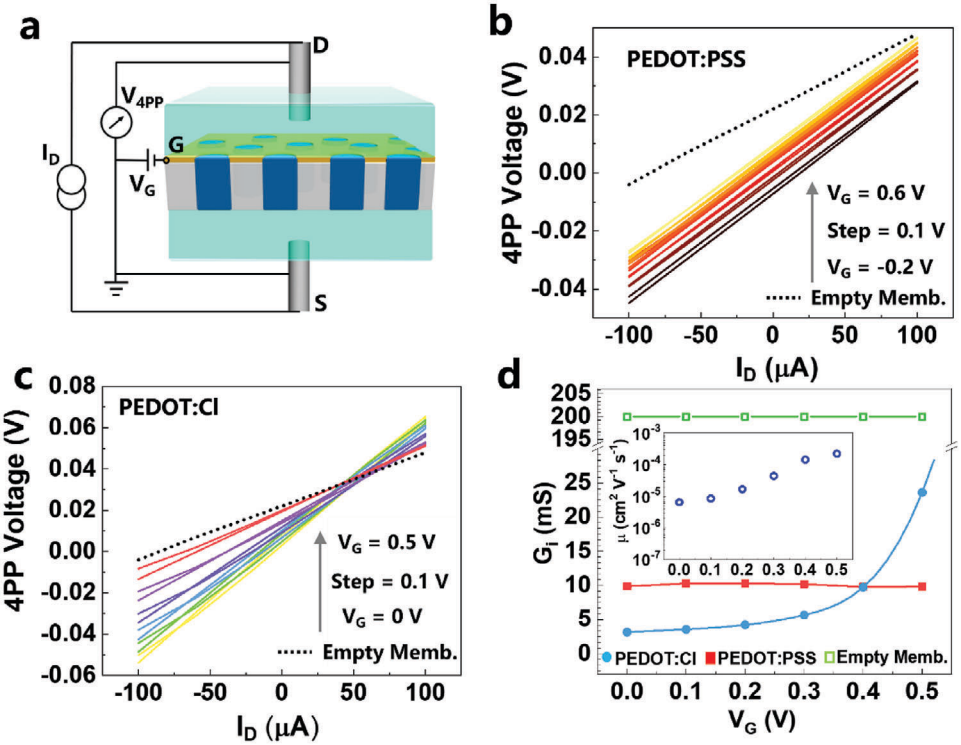

Figure 5. Investigation of ionic transport in OMIEC filled nanopores. a) Scheme showing the measurement circuit of the ionic transistor. A single metal layer is used to contact the OMIEC nanopores as a gate; a 4-point-probe circuit is installed for measuring the potential difference across the membrane while an ionic current is sourced through the nanopores using salt bridges acting as source and drain electrodes. b,c) Measured voltage drop V_{4pp} across the membrane as a function of ionic current I_D for different gate potentials. PEDOT:PSS b) and PEDOT:Cl c) were used as OMIEC channel material. d) Channel conductance G_i of PEDOT:Cl and PEDOT:PSS as a function of gate potential. For PEDOT:Cl a significant modulation is observed and the differential ionic mobility of Cl^- ions is calculated (inset).

A different observation is made in PEDOT:Cl filled nanoporous membranes which were prepared by using NaCl as electrolyte salt during the electrodeposition process (see data on PEDOT:Cl filled nanoporous in Figure S4, Supporting Information). This OMIEC material includes fewer ions during the electrodeposition. The measured ionic current characteristics are shown in Figure 5c (the comparisons of the different OMIECs-filled membranes are present in Figure S5, Supporting Information). Now, one observes a significant effect of the gate potential on the slope of the ionic current – voltage curves. At 0 V applied to the gate, the pores show a steep *I–V* curve demonstrating a low ionic conductivity. When the gate potential is changed to positive values, a reduction in slope is observed that demonstrates an increase in conductivity. The increased conductivity is explained by chloride anions entering the channel to counterbalance the hole charges induced with the positive gate potential on the PEDOT chains. The semiconducting polymer is doped (oxidized) and the concentration of chloride ions increases, giving rise to a higher ionic carrier concentration with a measurable increase in ionic conductivity. The data demonstrates that the third electrode in our measurement (the gate) allows to modulate the ionic transport through the nanochannel. Accordingly, we term such a device an ionic transistor. However, we note, that the gate action does not permit to fully switch-off the ionic transport as would be possible in a normal electronic field effect transistor.

From the gating effect on the ionic conductivity G_m, we can estimate the ionic mobility μ_i following a formalism similar to volumetric gating in OECTs (see Section S2, Supporting Information). The linear ionic current curves confirm that the linear channel approximation is valid and Figure 5d shows the obtained conductivities G_m as a function of gate voltage. From the slope of this curve, we calculate the ionic differential mobility with

$$\mu_i = \frac{L^2}{C}\frac{d\,G}{d\,V_G} \tag{2}$$

in which C is the capacitance determined with EIS and L the thickness of the nanoporous membrane. A maximum value of $\mu_i = 3 \times 10^{-4}$ cm^2 V^{-1} s^{-1} is observed that is comparable to the ionic mobility of chloride anions in pure water as 5.7×10^{-4} cm^2 V^{-1} s^{-1} [22] and hence underlines the good ionic transport properties of the OMIEC material. However, we note that the conductivity does not show a linear increase with gate voltage and also it is not possible to inhibit completely the ionic conductivity through the nanochannel by applying negative gate voltages. Such differences from the ideal transistor behavior rely on the physical-chemical nature of ionic transport: In contrast to the bandgap in semiconductors, there is no energy interval in the electrochemical potential in which ions are forbidden to enter the OMIEC channel. Even though there is no electrostatic driving force, a smaller concentration of cations and anions will always

enter from the electrolyte due to entropic reasons. Another critical effect regards electroswelling. The increase in cationic concentration causes the uptake of water and swelling of the OMIEC material. The increase in water volume inside the pore is likely to enhance ionic conductivity explaining the superlinear increase of gate voltage.

3. Conclusion

In this work we present the fabrication of OMIEC filled nanochannels by the electropolymerization of EDOT monomers inside a nanoporous polycarbonate membrane. We use the method to build a novel vertical nanochannel OECTs. The approach provides an alternative to the common thin film approach used in OECT fabrication and introduces a template-based fabrication scheme to obtain microstructured OECTs. The vertical nanochannel OECTs with a channel length of 10 µm show a high transconductance of 5.6 mS comparable to state-of-the-art thin film devices.[5,23] The hole carrier mobility of (5.1 ± 0.42) x 10^{-3} cm^2 V^{-1} s^{-1} is below values obtained in thin film OECTs,[24] but is comparable to values obtained in self-organized electrochemical transistors based on electropolymerization.[14,25] Our template based approach is an additive process and compatible with wet and printing based fabrication steps allowing to avoid photolithography for low-cost and large area applications.

The unconventional nanoporous, vertical OECT architecture enables to exploit ionic as well as electronic transport properties of OMIEC materials. It allows to prepare OECT channels that are permeable to ions and water. We exploit the effect to demonstrate a novel type of ionic transistor in which the ionic conductivity of the nanochannel is gated by an electrical potential applied to the nanopore membrane. In literature, a similar gating effect was observed in nanofluidic diodes covered with a conducting polymer layer.[26] Interest in such ionic devices is emerging as they emulate properties of voltage gated ion-channels found in biological membranes. In our device we achieve the gating effect in a symmetric design relying on the modulation of the ion concentration in the channel. The developed ionic transistor enables to quantify ionic differential mobilities inside the active channel thus providing a novel tool to investigate ionic transport in OMIEC materials. For future research, we envision that the nanoporous OMIEC channels will open novel pathways towards mixed ionic and electronic circuits, that are fabricated without photolithography and that can be stacked to yield 3D architectures.

4. Experimental Section

Materials and Solutions: The electrodeposition solution was prepared by dissolving 10 mM 3,4-ethylenedioxythiophene (EDOT, Sigma Aldrich) with 0.1 mM poly(sodium 4-styrenesulfonate) (NaPSS, average Mw≈70 000, Sigma Aldrich) for PEDOT:PSS or 0.1 M NaCl for PEDOT:Cl in deionized water, and stirred 1 h to obtain a homogeneous transparent solution.

Electrodeposition of Polymer Nanochannels: The nanoporous membranes (ion track-etch membrane, Cytiva) used as the substrates were based on polycarbonate, the size of nanopores is 800 nm, and the diameter of the membranes is 13 mm. Before the conductive polymer electrodeposition, 30 nm of Cr (to enhance the attachment of Au to the membrane) and 50 nm layer of Au were deposited on one side of the membranes by thermal evaporation. The membranes were fixed by sticking their Au/Cr coated side on the flat PDMS layer. In order to define the deposited area of the polymers on membrane, each membrane was shielded with another PMDS film having a 5 mm window where the membrane contact the electrodeposition solution. All the membranes were treated with air plasma to enhance the hydrophilicity and mounted in an electrochemical cell; then, the membranes were sonicated in the electrodeposition solution at 30 °C. These operations facilitated the solution to enter the nanopores in the membranes. Before electrodeposition, the nitrogen was fluxed for 15 min in the sealed electrochemical cell to remove the oxygen. The electropolymerization was carried out with Autolab potentiostat AUT50662 (Metrohm) controlled by NOVA software, and the Ag/AgCl wire and Pt wire were used as the reference electrode and the counter electrode, respectively. For the electrodeposition of PEDOT:PSS, the cyclic voltammetry was executed between −0.3 and 1.2 V at a scan rate of 0.025–0.05 V s^{-1}. PEDOT:Cl pores filling was performed through a fixed voltage (1.2 V) coulometric procedure. After electrodeposition, the membranes were rinsed with DI water to remove the residual electrolyte.

Electrochemical Characterization: The electrochemical data for the charge, cyclovoltammetry, and electrochemical impedance spectroscopy (EIS) were recorded in the electrodeposition solution with the Autolab potentiostat AUT 50 662 (Metrohm) controlled by NOVA software.

Morphology Characterization: The morphology of both sides was analyzed by AFM (Park NX10 AFM) with tapping mode in the atmosphere. The morphology of the cross section and EDX mapping analysis was observed with SEM (Cambridge Stereoscan 360). The accelerating voltage was 20 kV, the cross section samples were obtained by cracking the membranes while they were frozen in liquid nitrogen.

Electrical Characterization of OECTs: To characterize the electronic transport, another layer of Au/Cr was evaporated on the other side of the membrane, this couple of electrodes were employed as the source and drain. The electrical characterizations of the transfer, output, I_D (t) measurements were performed with the source measure unit B2912A (Keysight). The evaporated Au/Cr on both sides were the source and drain, the PBS solution was used as the electrolyte, and the Ag/AgCl electrode pellet (1.0 mm, E205, Warner) was employed as the gate.

Characterization of Ionic Transistors: The OMIEC filled nanoporous membrane was inserted in a measurement cell and on both sides in contact with 1x PBS electrolyte (details of the measurement are provided in Figure S6, Supporting Information). The area in contact with the electrolyte was confined by a silicone O-ring of 5.0 mm diameter. A source measure unit (SMU, Keysight B2912) was used to source a current through the membrane using PBS/agarose salt bridges. The voltage drop across the nanoporous membrane was measured with a 4-point-probe configuration using two Ag wires coated with AgCl. The potential of the OMIEC filled membrane was controlled with the 2nd SMU channel connected with a copper wire and silver paste to the gold coating of the membrane. To characterize the membranes, the SMU was programmed to sweep the current from −100 to 100 µA and back while measuring the voltage drop. The measurement was repeated for different gate voltages.

Supporting Information

Supporting Information is available from the Wiley Online Library or from the author.

Acknowledgements

C.Z. and L.M. contributed equally to this work. C.Z. gratefully acknowledges the Fundamental Research Funds for the Central Universities and Graduate Student Innovation Fund of Donghua University (CUSF-DH-D-2021004). The research leading to these results has received funding from the European Union - NextGenerationEU through the Italian Ministry of University and Research under PNRR - M4C2-I1.3 Project PE_00000019 "HEALITALIA" to Tobias Cramer CUP J32G19001080005.

Conflict of Interest

The authors declare no conflict of interest.

Data Availability Statement

The data that support the findings of this study are available from the corresponding author upon reasonable request.

Keywords

nanotemplated deposition, nanochannel, organic electrochemical transistors, organic mixed ionic electronic conductors, track-etched membranes, vertical transistors

Received: November 17, 2023
Published online:

[1] a) C. Pitsalidis, A.-M. Pappa, A. J. Boys, Y. Fu, C.-M. Moysidou, D. Van Niekerk, J. Saez, A. Savva, D. Iandolo, R. M. Owens, *Chem. Rev.* **2022**, *122*, 4700; b) M. Berggren, A. Richter-Dahlfors, *Adv. Mater.* **2007**, *19*, 3201; c) D. T. Simon, E. O. Gabrielsson, K. Tybrandt, M. Berggren, *Chem. Rev.* **2016**, *116*, 13009; d) F. Decataldo, I. Gualandi, M. Tessarolo, E. Scavetta, B. Fraboni, *APL Mater.* **2020**, *8*, 091103; e) F. Bonafè, F. Decataldo, I. Zironi, D. Remondini, T. Cramer, B. Fraboni, *Nat. Commun.* **2022**, *13*, 5423; f) H. Lee, S. Lee, W. Lee, T. Yokota, K. Fukuda, T. Someya, *Adv. Funct. Mater.* **2019**, *29*, 1906982.

[2] a) A. Campana, T. Cramer, D. T. Simon, M. Berggren, F. Biscarini, *Adv. Mater.* **2014**, *26*, 3874; b) V. Venkatraman, J. T. Friedlein, A. Giovannitti, I. P. Maria, I. Mcculloch, R. R. Mcleod, J. Rivnay, *Adv. Sci.* **2018**, *5*, 1800453.

[3] a) Y. Van De Burgt, A. Melianas, S. T. Keene, G. Malliaras, A. Salleo, *Nat. Electron.* **2018**, *1*, 386; b) J. Y. Gerasimov, R. Gabrielsson, R. Forchheimer, E. Stavrinidou, D. T. Simon, M. Berggren, S. Fabiano, *Adv. Sci.* **2019**, *6*, 1801339; c) J. Y. Gerasimov, D. Tu, V. Hitaishi, P. C. Harikesh, C.-Y. Yang, T. Abrahamsson, M. Rad, M. J. Donahue, M. S. Ejneby, M. Berggren, R. Forchheimer, S. Fabiano, *Adv. Sci.* **2023**, *10*, 2207023.

[4] A. Koklu, D. Ohayon, S. Wustoni, V. Druet, A. Saleh, S. Inal, *Chem. Rev.* **2022**, *122*, 4581.

[5] D. Khodagholy, J. Rivnay, M. Sessolo, M. Gurfinkel, P. Leleux, L. H. Jimison, E. Stavrinidou, T. Herve, S. Sanaur, R. M. Owens, G. G. Malliaras, *Nat. Commun.* **2013**, *4*, 2133.

[6] F. Torricelli, D. Z. Adrahtas, Z. Bao, M. Berggren, F. Biscarini, A. Bonfiglio, C. A. Bortolotti, C. D. Frisbie, E. Macchia, G. G. Malliaras, I. McCulloch, M. Moser, T. Q. Nguyen, R. M. Owens, A. Salleo, A. Spanu, L. Torsi, *Nat. Rev. Methods Primers* **2021**, *1*, 66.

[7] J. T. Friedlein, R. R. Mcleod, J. Rivnay, *Org. Electron.* **2018**, *63*, 398.

[8] D. Khodagholy, M. Gurfinkel, E. Stavrinidou, P. Leleux, T. Herve, S. Sanaur, G. G. Malliaras, *Appl. Phys. Lett.* **2011**, *99*, 163304.

[9] a) W. Huang, J. Chen, Y. Yao, D. Zheng, X. Ji, L.-W. Feng, D. Moore, N. R. Glavin, M. Xie, Y. Chen, R. M. Pankow, A. Surendran, Z. Wang, Y. Xia, L. Bai, J. Rivnay, J. Ping, X. Guo, Y. Cheng, T. J. Marks, A. Facchetti, *Nature* **2023**, *613*, 496; b) M. Abarkan, A. Pirog, D. Mafilaza, G. Pathak, G. N'kaoua, E. Puginier, R. O'connor, M. Raoux, M. J. Donahue, S. Renaud, J. Lang, *Adv. Sci.* **2022**, *9*, 2105211.

[10] E. J. Choi, N. P. Drago, N. J. Humphrey, J. Van Houten, J. Ahn, J. Lee, I. D. Kim, A. F. Ogata, R. M. Penner, *Mater. Today* **2023**, *62*, 129.

[11] a) F. A. Plamper, *Colloid Polym. Sci.* **2014**, *292*, 777; b) H. S. Varol, T. Herberger, M. Kirsch, J. Mikolei, L. Veith, V. Kannan-Sampathkumar, R. D. Brand, C. V. Synatschke, T. Weil, A. Andrieu-Brunsen, *Chem. Mater.* **2023**, *35*, 9192.

[12] a) H. S. White, G. P. Kittlesen, M. S. Wrighton, *J. Am. Chem. Soc.* **1984**, *106*, 5375; b) J. Lee, S. Chhatre, P. Sitarik, Y. Wu, Q. Baugh, D. C. Martin, *ACS Appl. Mater. Interfaces* **2022**, *14*, 42289; c) D. A. Koutsouras, F. Torricelli, P. Gkoupidenis, P. W. M. Blom, *Adv. Mater. Technol.* **2021**, *6*, 2100732.

[13] a) J. Brodský, I. Gablech, L. Migliaccio, M. Havlicek, M. J. Donahue, E. D. Glowacki, *ACS Appl. Mater. Interfaces* **2023**, *15*, 27002; b) R. Rybakiewicz-Sekita, M. Gryszel, G. Pathak, R. Ganczarczyk, M. J. Donahue, E. D. Glowacki, *J. Mater. Chem. C* **2022**, *10*, 17208; c) D. A. Koutsouras, F. Torricelli, P. W. M. Blom, *Adv. Electron. Mater.* **2022**, *9*, 2200868.

[14] K. Janzakova, M. Ghazal, A. Kumar, Y. Coffinier, S. Pecqueur, F. Alibart, *Adv. Sci.* **2021**, *8*, 2102973.

[15] S. Carli, M. Bianchi, M. Di Lauro, M. Prato, A. Toma, M. Leoncini, A. De Salvo, M. Murgia, L. Fadiga, F. Biscarini, *Front. Mater.* **2022**, *9*, 1063763.

[16] I. Gualandi, M. Tessarolo, F. Mariani, D. Arcangeli, L. Possanzini, D. Tonelli, B. Fraboni, E. Scavetta, *Sensors* **2020**, *20*, 3453.

[17] J. Ji, Y. Fu, J. Wang, P. Y. Chen, D. Han, Q. Zhang, W. Zhang, S. Sang, X. Yang, Z. Cheng, *J. Mater. Chem.* **2020**, *C8*, 11499.

[18] a) I. Blaszczyk-Lezak, V. Desmaret, C. Mijangos, *eXPRESS Polym. Lett.* **2016**, *10*, 259; b) Y. Zhou, N. Shida, Y. Koizumi, K. Endo, I. Tomita, S. Inagi, *Macromolecules* **2020**, *53*, 8123; c) A. Rath, P. Theato, *Adv. Funct. Mater.* **2019**, *30*, 1902959.

[19] C. Mijangos, J. Martin, *Polymers* **2023**, *15*, 525.

[20] T. Ma, J. M. Janot, S. Balme, *Small Methods* **2020**, *4*, 2000366.

[21] A. V. Volkov, K. Wijeratne, E. Mitraka, U. Ail, D. Zhao, K. Tybrandt, J. W. Andreasen, M. Berggren, X. Crispin, I. V. Zozoulenko, *Adv. Funct. Mater.* **2017**, *27*, 1700329.

[22] S. Koneshan, J. C. Rasaiah, R. M. Lynden-Bell, S. H. Lee, *J. Phys. Chem. B* **1998**, *102*, 4193.

[23] J. Rivnay, P. Leleux, M. Ferro, M. Sessolo, A. Williamson, D. A. Koutsouras, D. Khodagholy, M. Ramuz, X. Strakosas, R. M. Owens, C. Benar, J.-M. Badier, C. Bernard, G. G. Malliaras, *Sci. Adv.* **2015**, *1*, 1400251.

[24] F. Bonafè, F. Decataldo, B. Fraboni, T. Cramer, *Adv. Electron. Mater.* **2021**, *7*, 2100086.

[25] S. Demuru, B. P. Kunnel, D. Briand, *Biosens. Bioelectron.: X* **2021**, *7*, 100065.

[26] a) G. Pérez-Mitta, W. A. Marmisollé, C. Trautmann, M. E. Toimil-Molares, O. Azzaroni, *Adv. Mater.* **2017**, *29*, 1700972; b) G. Laucirica, Y. Toum Terrones, M. F. P. Wagner, V. M. Cayón, M. L. Cortez, M. E. Toimil-Molares, C. Trautmann, W. Marmisollé, O. Azzaroni, *Nanoscale* **2023**, *15*, 1782.